



Title	Column and film lifetimes in bubble-induced two-liquid flow
Author(s)	Natsui, Shungo; Nashimoto, Ryota; Nakajima, Daiki; Kikuchi, Tatsuya; Suzuki, Ryosuke O.
Citation	Physical Review E, 97(6), 062802 https://doi.org/10.1103/PhysRevE.97.062802
Issue Date	2018-06-18
Doc URL	http://hdl.handle.net/2115/71348
Rights	©[2018] American Physical Society
Type	article
File Information	PhysRevE.97.062802.pdf



[Instructions for use](#)

Column and film lifetimes in bubble-induced two-liquid flow

Shungo Natsui,¹ Ryota Nashimoto,² Daiki Nakajima,¹ Tatsuya Kikuchi,¹ and Ryosuke O. Suzuki¹

¹*Faculty of Engineering, Hokkaido University, Kita 13 Nishi 8, Kita-ku, Sapporo 060-8628, Japan*

²*Saganoseki Smelter & Refinery, Pan Pacific Copper Co., Ltd., 3-3382 Saganoseki, Oita 879-2201, Japan*



(Received 6 April 2018; published 18 June 2018)

We investigated the transient behavior of immiscible two-liquid interfaces initiated by a single rising gas bubble and characterized by liquid “column” and “film” morphologies. To analyze the effect of the buoyancy force, viscosity, and interfacial tension on these morphologies, the single-solution density was controlled continuously by association with the rising velocity of the bubble. It was observed that the extension of the liquid column further into the upper liquid phase owing to the wake flow under the bubble is driven by the buoyancy force, with the velocity decreasing gradually with the distance between the bubble and the liquid-liquid interface. Based on this mechanism, we determined that a strong dimensionless correlation exists between the lifetime of the column and the physical properties of the two liquid phases. On the other hand, gravitational drainage does not affect the film lifetime. However, marginal pinching is dominant, probably owing to the existence of a surface tension gradient between the film and the meniscus.

DOI: [10.1103/PhysRevE.97.062802](https://doi.org/10.1103/PhysRevE.97.062802)

I. INTRODUCTION

During high-temperature extractive metallurgical processes, a two-liquid-phase system consisting of a metal-rich phase and a less-dense slag phase is produced. The primary purpose of this system is to concentrate the metal phase into a form suitable for further refining and to efficiently remove the gangue materials as molten slag. Given the immiscibility of the two liquids typically involved, stirring is usually achieved through a gas flow. A “thin liquid metal film” is formed initially at the interface because of a rising gas bubble, resulting in a “liquid metal column,” which extends into the slag phase, owing to the wake flow under the bubble (Fig. 1) [1]. To enhance the reaction efficiency of the two liquids, the interfacial area between the molten metal and the slag phase must be increased. One way of achieving this is to emulsify the lower metal phase into the upper slag phase in the form of “metal droplets” [2,3]. However, the dispersed metal droplets become entrapped within the molten slag, which can result in financial losses if the slag containing the product metals is discarded without further treatment [4]. Since the efficiency of the base metal production process contributes significantly to the CO₂ emissions involved, the deformation of this immiscible two-liquid-phase interface must be controlled.

The interfacial deformation scenario resulting from a single rising bubble at a liquid-liquid interface can be described as follows. Because of gravity or capillary force, liquid 1 flows down into the bubble cap, leading to a thinner “film” [5]. In contrast to the case during film drainage, the wake of the rising bubble expands the “column” attracted upward by the bubble. The dynamic balance between the buoyancy force and the liquid-liquid interfacial tension determines the thickness of the column [6–8]. The height of the column generated by this movement increases steadily until a “neck” is formed, with droplets subsequently generated by rupturing of the neck because of the Plateau-Rayleigh instability. A hole eventually

nucleates in the film and propagates concentrically [9,10]. The question of when and where the column and film will burst is relevant to droplet generation, since their lifetimes determine the average thickness and interfacial area at the time of bursting, and thus the droplet size distribution, while the position of the nucleation point affects the dispersion of these droplets in the upper liquid phase.

The shape of the bubble directly influences film drainage based on both the orientation of the film with respect to the direction of gravity and the capillary pressure induced by the curvature of the interface. It also determines the bursting dynamics via column extension and the curvature of the cap. Liquid film drainage has already been studied intensively in the case of foams using two-dimensional configurations and implicitly assuming symmetrical revolution or horizontal translational invariance in a “static bubble,” which would be located near the free surface of the liquid and extremely slow compared with an upwardly flowing one [11–14]. However, this condition cannot be used to elucidate with precision the drainage dynamics in the case of bubbles wherein convection motion plays a first-order role.

To understand the dynamic behavior of a single gas bubble induced by a liquid-liquid interface, several studies based on direct optical observations, as well as numerical studies of interfacial flow, have been performed for a wide range of conditions [15–17]. Generally, room-temperature media such as water, oil, and mercury have been used to perform nondimensional analyses of liquid-liquid-gas systems [18]. Further, an additional rupture phenomenon wherein an elongated metal column is formed by two or three bubbles passing through the interface has also been reported in the case of a molten tin–molten salt system [19,20]. In this case, it was found that the liquid-liquid interfacial deformation behavior induced by a single rising bubble depends primarily on the physical properties of each liquid, such as density, viscosity, and interfacial tension. Although it has been suggested that

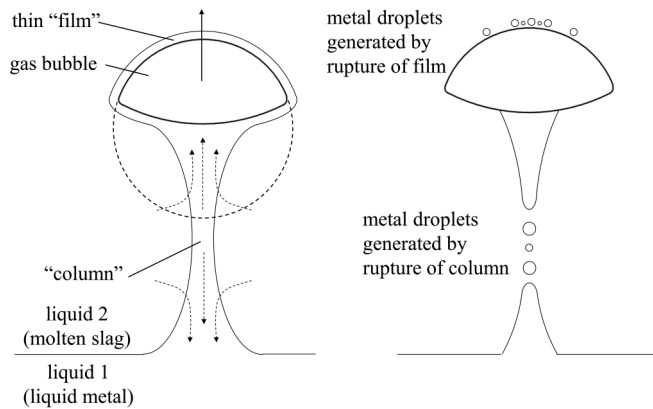


FIG. 1. Schematic diagram of a bubble passing through the interface between two liquids.

even a small change in the Bond number (or Eötvös number) and the Laplace number (or Ohnesorge number) considerably affects the interfacial shape, even in similar-material systems, it remains unclear as to which property primarily determines the column and film lifetimes. This is because, so far, it has not been possible to analyze the influence of individual physical properties. In this study, to simulate the various flow modes corresponding to continuous changes in the interfacial tension–gravity force ratio, we focused on controlling the density of a single liquid. For this, we employed a sodium polytungstate (SPT) solution–silicone oil (SO) system to elucidate the effect of a linear change in the density on the column and film lifetimes. A heavy-liquid solution was prepared by dissolving SPT in distilled water, and the solution density was changed continuously by varying the SPT concentration. The maximum attainable density of the solution in water at room temperature (293 K) was 3100 kg/m^3 .

II. METHODS

Figure 2 shows the experimental setup used. The experiments were performed in an air-conditioned room at a fixed temperature of 293 K. First, an acrylic tank (inner dimensions: $0.040 \times 0.090 \times 0.295 \text{ m}$; with this tank design, the wall effect does not affect bubbles and the thin film is easy to observe [21,22]) was filled with the two liquid phases (height of each phase: 0.090 m). The aqueous SPT solution was the lower liquid phase (liquid 1), while SO (KF-96-10cs,

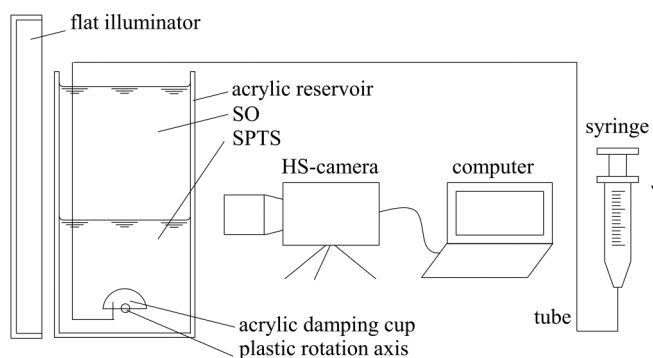


FIG. 2. Schematic diagram of experimental setup.

Shin-Etsu Chemical Co., Ltd.) was the upper liquid phase (liquid 2). Heavy-liquid solutions of different densities were prepared by dissolving SPT ($\text{Na}_6[\text{H}_2\text{W}_{12}\text{O}_{40}]$ in H_2O , Measure Works Co., Ltd.) in distilled water. In addition, to be able to analyze the film rupture time (see Sec. IV), several solutions were prepared using glycerol (GLY, $\text{C}_3\text{H}_8\text{O}_3$ in H_2O , Wako Chemical Co., Ltd.) or linear alkylbenzene sulfonate (LAS, $\text{C}_{18}\text{H}_{29}\text{NaO}_3\text{S}$ in H_2O , Wako Chemical Co., Ltd.) as liquid 1. Table I shows the physical properties of each solution [23–25]. The surface tension and interfacial tension were measured by the pendant drop method using an optical contact angle meter (DM-501, Kyowa Interface Science Co., Ltd.). Table I also lists the surface tension and interfacial tension for the various interfacial shapes, as determined based on the obtained images using the Young-Laplace method. Next, a constant volume of air was injected through a glass tube using a syringe pump. The air was trapped within a hemispherical plastic cup (inner diameter: 0.026 m). To this cup, a nichrome wire that could be rotated by 180° was attached to allow a single bubble to rise. The bubble volume was controlled to be $0.5 \times 10^{-6} \text{ m}^3$ to $5.0 \times 10^{-6} \text{ m}^3$ using the syringe pump. The changes in the interface were recorded using a high-speed video camera (FASTCAM, Photron Co., Ltd.) at a rate of 2000–10 000 frames per second and a resolution of 1024×1024 pixels. For each image captured, the position of the interface of each phase was analyzed using image processing software (PFV VIEWER and IMAGEJ). All the measurements were repeated at least five times under each condition. Using this procedure, we observed that the rising bubble modified the SPT-SO interface by pulling the SPT phase upward through the interface.

III. COLUMN LIFETIME

A. Experimental results

Figure 3 shows the obtained snapshots of a single bubble rising through the liquid 1 (water)–liquid 2 (SO) interface. Further, when the bubble passed through the liquids 1-2 interface, a thin film of liquid 1 was formed on the rising bubble and a wake structure was formed below the bubble. At this time, a film of liquid 1 was formed around the cap of the bubble. This film ruptured as it floated further away, and the bubble in liquid 2 was exposed. A column of liquid 1 was formed behind the floating bubble. Figure 4 shows the behavior of the bubbles passing through the various liquid 1 (SPT solution)–liquid 2 (SO) interfaces. The column immediately below the bubble became narrower as the density of liquid 1 was increased. A thicker column was

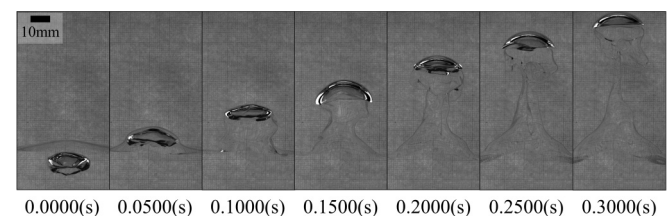


FIG. 3. Snapshots of a single air bubble with a constant volume ($2.0 \times 10^{-6} \text{ m}^3$) rising through a distilled water–SO interface.

TABLE I. Physical properties of solution components at room temperature (293 K).

	SO	No. 1 (Water)	No. 2 (SPT)	No. 3 (SPT)	No. 4 (SPT)	No. 5 (SPT)	No. 6 (SPT)	No. 7 (SPT)	No. 8 (GLY)	No. 9 (LAS)	No. 10 (LAS)
Density (kg m^{-3})	935	998	1250	1500	1750	2000	2500	3000	1222	998	998
Viscosity (mPa s)	9.35	1.0	1.2	1.4	2.0	3.1	10.2	38.1	109	1.0	1.0
Surface tension (mN m^{-1})	20.1	72.8	73.5	71.7	74.4	71.5	77.2	73.4	66.8	51.5	35.5
Interfacial tension between SO and component (mN m^{-1})		49.3	42.5	44.8	43.3	44.9	44.6	47.1	33.1	27.2	9.9
Capillary length (m)	0.0145	0.0267	0.0240	0.0216	0.0204	0.0187	0.0173	0.0154	0.0231	0.0224	0.0186

generated with a decrease in ρ_1 at $t = 0.3000$ s. The lifetime was defined as the time required for the column to rupture from when the bubble apex first reached the initial two-liquid interface. These results are summarized in Table II, and Fig. 5 shows the relationship between the column lifetime and bubble volume. With an increase in the bubble volume, the column lifetime also increased. Based on this result, we propose the following hypothesis. The initial form of the column depends on the pulling force generated by the buoyancy of the bubble, whereas the stretched column in liquid 2 sinks because of a sedimentation force arising from the difference in the densities of the two liquids. In the case of small bubble volumes ($V_b < 1.0 \times 10^{-6} \text{ m}^3$), the column lifetime decreased with an increase in ρ_1 . Therefore, the shape and lifetime of the column are determined by the balance between the interfacial force and the sedimentation force. With an increase in ρ_1 , the sedimentation force becomes larger, and the width of the column and the lifetime are reduced. However, this was not the case for

high- V_b conditions. At $V_b = 5.0 \times 10^{-6} \text{ m}^3$, the lifetime is the largest for No. 1, but the values oscillate for No. 2–7. In addition, in the case of liquid-liquid systems, wake shedding is known; i.e., wakes that aperiodically discharge vorticity, typically with convoluted geometry, are initially axisymmetric but eventually become unsteady and asymmetric with the onset of a turbulent wake [26]. Despite this turbulence, the bubble size exhibits a consistent relationship with the average column lifetime, and this trend was reproducible. Further, the bubble size was not correlated with the nonaxisymmetry of the column. Considering the capillary length, $\lambda_c = \sqrt{\sigma/\rho g}$, the projected bubble length would be greater than λ_c in the high- V_b region. Thus, the bubble could no longer be spherically approximated based on its deformation. In the case of $V_b > 1.0 \times 10^{-6} \text{ m}^3$, the interfacial deformation would be dominated by inertia and not by the interfacial force, which may influence the bursting position of the column and its maximum length.

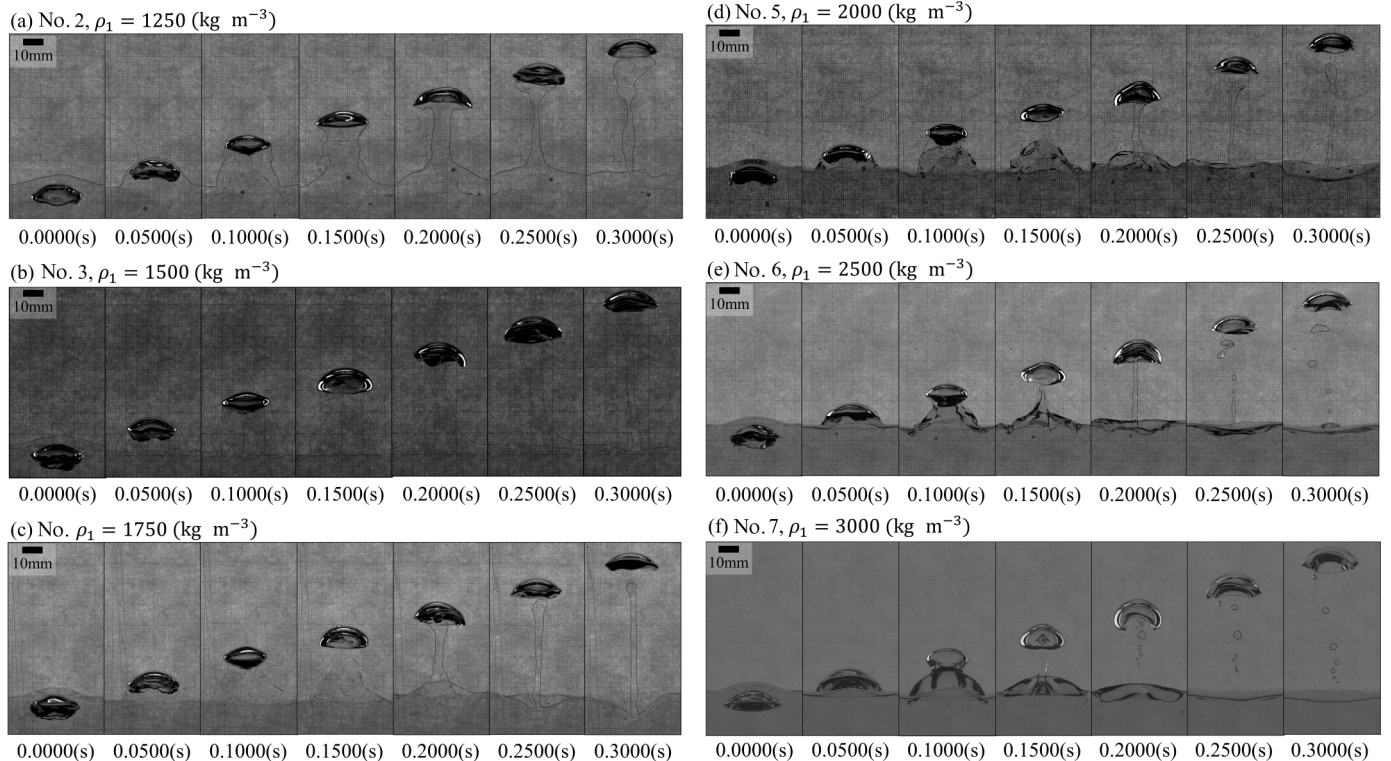


FIG. 4. Snapshots of single air bubbles with a constant volume ($2 \times 10^{-6} \text{ m}^3$) rising through SPT solution–SO interfaces. As the refractive indices of the SPT solution and SO are approximately equal, auxiliary lines have been added to help readers identify the SPT solution–SO interfaces.

TABLE II. Column lifetimes (unit: s).

Volume (ml)	No. 1	No. 2	No. 3	No. 4	No. 5	No. 6	No. 7	No. 8
0.5		0.2184	0.2147	0.1726	0.1424		0.1727	0.3201
1.0	0.3141	0.2916	0.2427	0.2487	0.2264	0.1793	0.1903	0.4549
2.0	0.4693	0.3270	0.3573	0.3236	0.2472	0.2052	0.2196	0.4981
3.0	0.5154	0.3693	0.3782	0.3582	0.3127	0.2669	0.2687	0.5599
4.0	0.5486	0.3808	0.3846	0.4191	0.3329	0.2481	0.2821	0.5671
5.0	0.5840	0.4080	0.3912	0.4421	0.3722	0.2590	0.2943	0.5415

B. Dimensional analysis

Through dimensional analysis, we derived a physical model for the column lifetime based on the hypothesis described in the previous section. When a bubble rises through liquid 1 toward the interface between two liquids, namely, liquids 1 and 2, the following three phenomena occur. The first is the rising of the bubble because of the buoyancy force, such that the velocity of the bubble decreases with the distance between it and the liquid-liquid interface [27]. As a result, the lower liquid column penetrates the upper liquid phase with the bubble. Second, because of drainage, a film of liquid 1 is formed between the bubble interface and liquid 2, with the thickness of the film decreasing with time. Similarly, drainage decreases the thickness of the liquid column. The third phenomenon is the rupturing of the film and column, resulting in the rapid generation of droplets. Based on the dimensional correlation, the parameters that control the column shape and lifetime can be determined. A characteristic of this analysis is that it allows for the simplification of the physical properties of each phase in order to analyze the dynamic behavior of the column. Although Bonhomme *et al.* [16] and Reiter and Schwerdtfeger [18] employed all the physical properties involved to determine a nondimensional correlation, estimating the column lifetime using this approach is a complicated process. The gas density and gas viscosity, as well as the surface tension between the gas and the two liquids, are not important for estimating the column lifetime, and we assumed that only the gas rising velocity influenced the column lifetime.

The shape of the column formed by a single bubble is mainly determined by the relative buoyancy force against the

interfacial tension between liquids 1 and 2. Here, we used the diameter of the single bubble, D , as the representative length and determined the ratio between these two forces, defined as the Bond number, as follows:

$$Bo = \frac{g\Delta\rho_{12}D^2}{\sigma_{12}}, \tag{1}$$

where $\Delta\rho_{12}$ is the difference in the densities of liquids 1 and 2, σ_{12} is the interfacial tension between liquids 1 and 2, and g is the acceleration due to gravity. Assuming axial symmetry, the column thickness L is a function of time t . The column thickness also depends on the interfacial viscosity. Visser *et al.* showed that when modeling multiviscosity fluids, using the mean of the friction factors corresponding to the interacting fluids improves the accuracy of the velocity profile [28]. The results for a multiphase Poiseuille flow test case showed that the harmonic mean of the fluid viscosities, corresponding to an interaction between two liquids, yields a velocity profile that is consistent with the analytically obtained profile. Thus, we employed the following expression: $\bar{\mu}_{12} = 2\mu_1\mu_2/(\mu_1 + \mu_2)$. Based on the Buckingham π theorem, which states that a physically meaningful equation involving a certain number n of physical variables can be rewritten in terms of a set of $p = n - k$ dimensionless parameters, $\pi_1, \pi_2, \dots, \pi_p$, constructed from the original variables. In this system, five physical quantities were assumed to be linked by the following relation:

$$f(t, U_t, D, L, g, \Delta\rho_{12}, \sigma_{12}, \bar{\mu}_{12}) = 0, \tag{2}$$

where t is time, U_t is the rising velocity of the single bubble in liquid 1, D is the bubble diameter, L is the column thickness, g is gravity, ρ is the density, σ is the interfacial tension, and μ is the viscosity. Using the π theorem, four dimensional parameters can be derived as $Bo, La, L/D$, and tU_t/D . The rising velocity can be estimated by tracking the top of the bubble at each time. The rising velocity was almost constant for each bubble volume when the bubble passed through the interface, as shown in Fig. 6(a), but the bubble rising velocity became smaller when located entirely in liquid 2, as shown in Fig. 6(b). We discuss the nondimensional correlation using this experimentally derived U_t value. Here, the dimensionless number $La (= Oh^{-2} = We^{-1}Re^2)$ is the Laplace number, which compares the viscous force to the inertial and capillary forces, as shown below:

$$La = \frac{\sigma_{12}\Delta\rho D}{\bar{\mu}_{12}^2}. \tag{3}$$

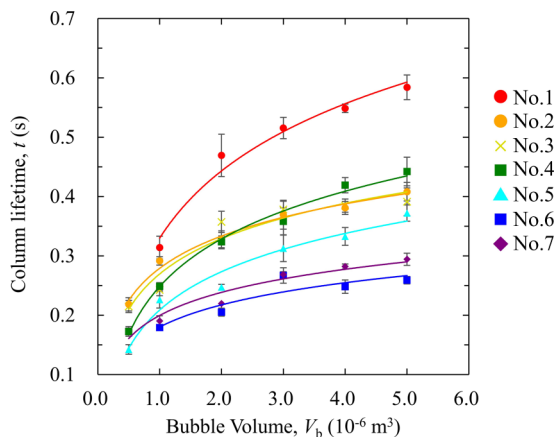


FIG. 5. Bubble-volume dependence of the SPT solution column lifetime.

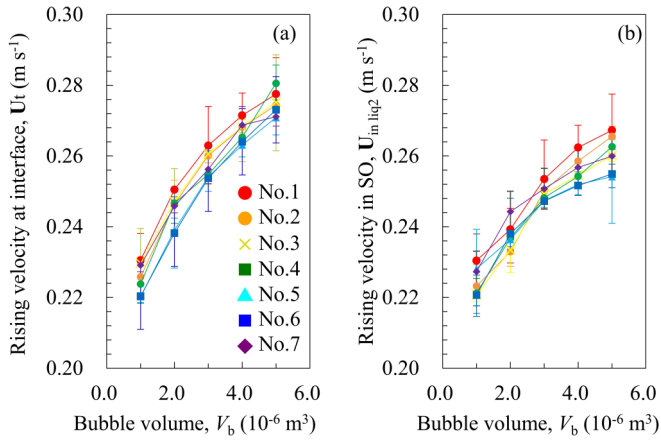


FIG. 6. Influence of bubble volume on the rising velocity of the bubble (a) at the interface and (b) in SO.

Then, Eq. (2) can be rewritten as [29]

$$\frac{L}{D} = f\left(Bo, La, \frac{tU_t}{D}\right). \quad (4)$$

Here, tU_t/D is the characteristic dimensionless time given as τ . Based on the correlation between L and D , we assumed the simplification of $L/D = \text{const}$. Thus, using the following three basic dimensions, length (l), time (t), and mass (m), Eq. (4) can be written using a proportionality constant k and index numbers as follows:

$$\tau = kLa^A Bo^B. \quad (5)$$

Figure 7 shows the column lifetimes for No. 1–8 in the absence of a surfactant. Based on parameter fitting, we obtained the following weak relationship: $A = 1/2$, $B = 1/3$, $k = 0.0024$. As the representative length of the projected surface of the bubble is larger than λ_c , the deformation cannot be ignored; thus, better fitting will be obtained by considering such morphology changes.

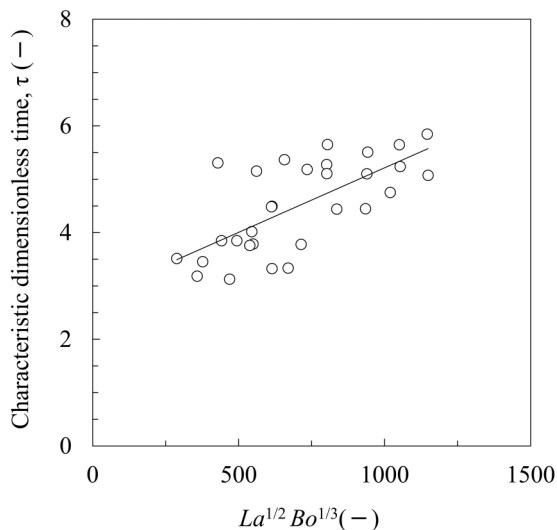


FIG. 7. Experimentally obtained nondimensional correlation between column lifetime and physical properties of liquids.

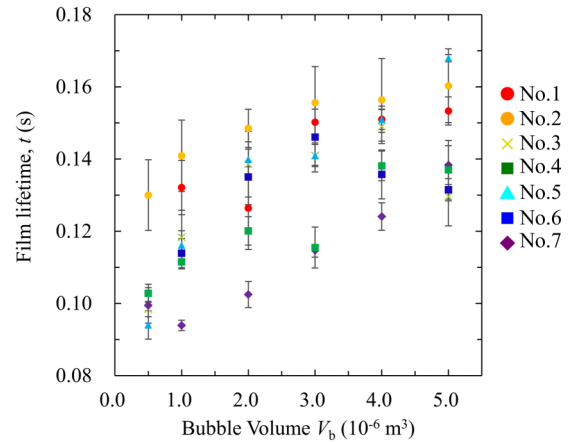


FIG. 8. Bubble-volume dependence of the SPT solution film lifetime.

IV. FILM LIFETIME

A. Experimental results

To estimate the film lifetime, we first assumed that the thinning of the film on the top of the bubble is due to the pressure imposed by the rising bubble and by the top interface, which resists further deformation once the shape of the fluid interface stops changing. However, the buoyancy force pulls the bubble upward while the capillary force pushes the interface downward. Consequently, the fluid in the film is squeezed. Based on this mechanism, it can be concluded that the greater the density of liquid 1, the higher the buoyancy force generated between liquids 1 and 2, resulting in a decrease in the film lifetime. Figure 8 shows the relationship between the bubble volume and film lifetime when the density of liquid 1 is varied. Although the lifetime tended to increase with the bubble volume, we did not find a simple relationship corresponding to the increase in the density of liquid 1, suggesting that the film lifetime is not strongly correlated to this liquid property. Therefore, the gravity force, as suggested by the mechanism described above, is not a significant factor affecting the film lifetime. Figure 9 shows the case where the viscosity and interfacial tension were varied. In the case of GLY, the viscosity was 109 times that of water. However, the film lifetime was lower than that in the case of water, regardless of the bubble diameter. Further, it was observed that the “drainage” mechanism alone, which is based on gravity, cannot explain the decrease in the film thickness. In the case of a “static bubble,” which would be moving very slowly near the free surface of the liquid, the smaller the area of the thin film as compared to the surface of the bubble, the faster the drainage [30,31]. In contrast, as observed in this study, when a bubble rises with deformation, the bubble size is not a dominant factor affecting the film lifetime, but the interfacial activity is. In other words, in the case of the LAS solution, the film lifetime increased sharply with an increase in the concentration. Further, the correlation between the film lifetime and the bubble diameter was weak in the case of the LAS-SO system. Hence, the effect of the change in the curvature of the bubble cap on the drainage rate could be ignored.

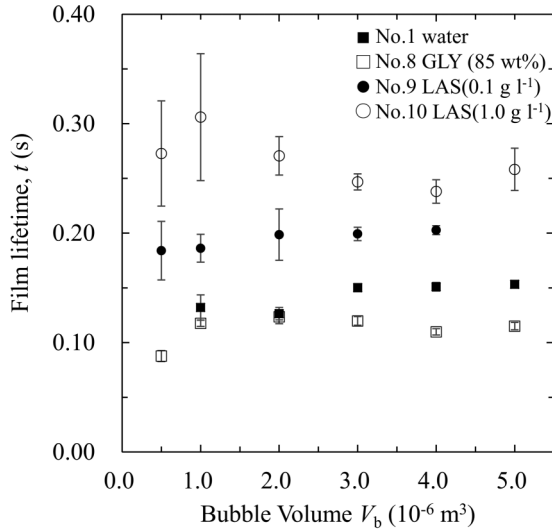


FIG. 9. Effect of solution type on the liquid film lifetime.

B. Drainage in the film

Based on the above-described results, it is likely that an additional film thinning mechanism, namely, “marginal regeneration,” which was introduced by Mysels *et al.* [32], is active in this system. This mechanism involves the formation of thin pinching zones in the film, probably owing to the existence of a surface tension gradient between the film and the meniscus [14,33]. Champougny *et al.* [5] proposed that in the case of a static bubble film, both factors responsible for rupturing—gravitational drainage and marginal regeneration—coexist under all conditions, with the former being dominant at high surfactant concentrations and the latter governing the bursting phenomenon at low concentrations. Considering this mechanism, the results of this study allow discussion of whether the film protection effect attributable to the surfactant is isotropic for a rising bubble.

Figure 10 shows representative dynamic behaviors of the liquid films in each liquid system. As shown in Figs. 10(a) and 10(b), in the system without the LAS solution, the bubble nucleation points are scattered. In contrast, in the LAS-SO system, the rupture site is at the apex portion. To explain this transition, Lhuissier and Villermaux proposed that marginal regeneration may be responsible for bubble rupturing at low concentrations, as rupturing at the apex in the case of higher concentrations is driven by gravitational drainage. This phenomenon can be characterized by the position of the rupture nucleation point, as follows [34]:

$$\Theta = \frac{\theta_{\text{rupt}} - \theta_{\text{min}}}{\pi/2 - \theta_{\text{min}}}. \tag{6}$$

This definition is depicted in Fig. 11(a), where the rupture angle, θ_{rupt} , varies from θ_{min} to $\pi/2$ because of the symmetry of the bubble with respect to the vertical axis. The displayed reduced rupture angle, Θ , values are averages for more than five bubbles under the same conditions (V_b and LAS concentration, C), with the error bar representing the standard deviation. With an increase in C , the position of the rupture site moves to the bubble apex, as shown in Fig. 11(b). Further, as shown in

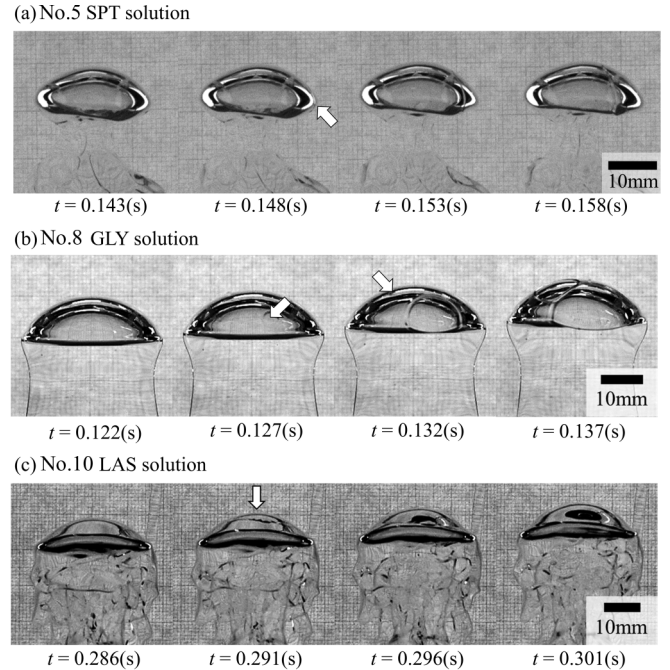


FIG. 10. Spontaneous bursting of various liquid films owing to rising of a single bubble ($3.0 \times 10^{-6} \text{ m}^3$). Rupture nucleation points are indicated by white arrows. The initial time is defined as the time when the bubble top reaches the initial interface between the two liquids. The corresponding error is $\pm 0.4 \text{ ms}$.

the Appendix, even though the critical micelle concentration (cmc) was estimated to be approximately 1 g l^{-1} , there was no notable change in Θ due to C . On average, Θ decreased when the surfactant concentration was reduced, consistent with the data reported by Champougny *et al.* [5]. This result suggests that the liquid flow in the film is not governed by the convective field formed by the rising bubbles with an increase in the surfactant concentration. In the absence of a surfactant, the drainage rate is not determined by the flow over the entire bubble cap. Instead, it is affected by fluctuations near the foot of the bubble, where the cap connects to the wake flow. Regardless of the value of C , Θ increased with an increase in V_b . As the radius of curvature of the vertex did not change noticeably with increasing V_b , any change can be presumed to be due to a simple decrease in θ_{min} . Thus, it still cannot be concluded that the deformation of the bubble influences the rupture site. However, it is obvious that the change in the low randomness of the burst angle of the film is attributable to the change in the form of flow in the film.

V. CONCLUSIONS

In this study, the effects of a single rising gas bubble pushed upward toward an interface between two immiscible liquids by gravity were investigated. First, we focused on the behavior of the interface between an SPT solution and SO to elucidate the effects of density on the flow characteristics. Using a high-speed camera, it was observed that after free rising of a single bubble, a liquid column and liquid film of the SPT solution form between the bubble and the SO phase. In addition, to characterize the lifetime of the liquid film, we

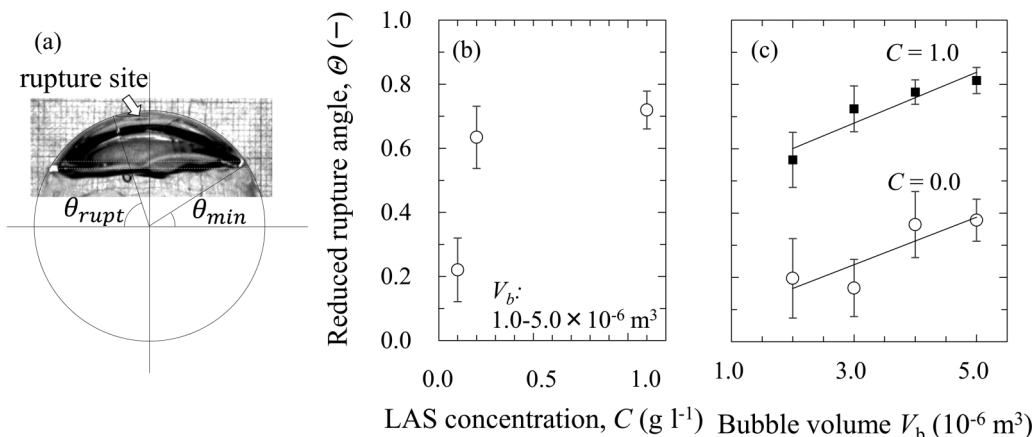


FIG. 11. (a) Definition of the rupture angle and minimum angle corresponding to the limit of the bubble foot, (b) effect of LAS concentration on the reduced rupture angle characterizing the position of the rupture nucleation point, and (c) effect of bubble volume on the reduced rupture angle for various LAS concentrations.

studied the dependence of the phenomena of drainage and film bursting around a floating bubble on the surfactant (LAS) concentration and bubble volume.

In the SPT solution–SO system, the lifetime of the liquid column increased with an increase in the bubble volume. In other words, the thickness of the liquid column depended on the projected area of the single bubble, while its drainage velocity was a function of the gravitational sedimentation force, interfacial tension, and viscous force. Further, the characteristic time indicated that there was a strong correlation between the Bo number and the La number.

In contrast, the liquid film lifetime was only weakly correlated to the bubble size and no association was observed with the Bo number. This behavior resulted from the fact that marginal regeneration, not gravitational drainage, was the primary factor responsible for film rupture. The mechanism of marginal pinching at the bubble foot and the associated convection motion in the bubble cap, known as marginal regeneration, both determine the bubble cap drainage rate and are responsible for puncturing of the bubble [35]. Further, we found that when a surfactant is present, gravity sedimentation becomes a primary factor in determining drainage, even when the rising bubble is deformed. The latter factor is responsible for bursting at the bubble foot at low concentrations, while the former factor is dominant at high surfactant concentrations and leads to hole nucleation at the apex. The generation efficiency of the marginal regeneration convection cell did not remain constant when the SPT concentration was varied, probably due to the strength of the interaction between the water molecules. At a sufficiently high surfactant concentration, the film thickness at the time of rupture was of the submicron scale, in keeping with a previous report [7], and was not greatly affected by the rising motion of the bubble.

ACKNOWLEDGMENTS

This study was supported by a Grant-in-Aid for Scientific Research (KAKENHI Grants No. 15K18250 and No. 18K14036). S.N. was partially supported by the Network Joint Research Center for Materials and Devices. We would

especially like to thank Dr. Takehiko Kumagai for valuable discussions on the experimental design of this study.

APPENDIX: CRITICAL MICELLE CONCENTRATION OF LAS SOLUTION

The critical micelle concentration (cmc) is one of the most important characteristics of a surfactant, in the case where the surfactant molecules added to a system begin to form micelles,

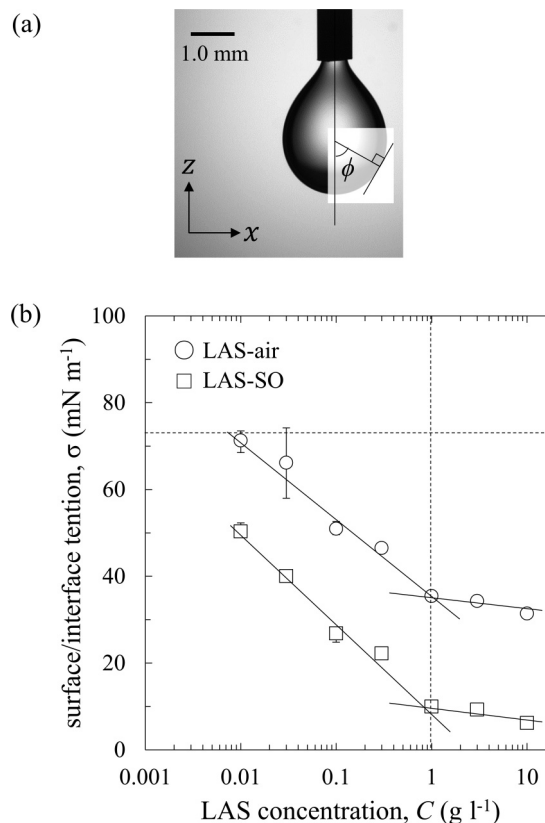


FIG. 12. (a) Hanging LAS droplet for determination of the interfacial tension using the pendant drop method. (b) Dependence of interfacial tension on LAS concentration.

and is determined by the change in the interfacial tension gradient. In this study, we measured the interfacial tension at each LAS concentration using the pendant drop method. Hanging droplets were extruded in the vertical direction from the tip of a capillary, and the interfacial tension was determined from the shape corresponding to the maximum volume. Figure 12(a) shows a single image of a hanging LAS droplet. The shape of the droplet interface can be described by the following Young-Laplace equation:

$$\frac{dx}{ds} = \cos \phi, \quad \frac{dz}{ds} = \sin \phi, \quad \frac{d\phi}{ds} = 2 + \beta z - \frac{\sin \phi}{x}, \quad (\text{A1})$$

where ϕ is the angle formed by the normal line of the interfacial curve and the vertical axis, and β is a shape factor [36]. Here,

β is defined using the principal curvature radius, b , of the interfacial curve of the hanging drop at the lowest point of the droplet, as follows:

$$\beta = \frac{\Delta\rho g b^2}{\sigma}. \quad (\text{A2})$$

Since $\Delta\rho$ is known, the interfacial tension σ can be calculated from the determined value of β . The dependence of the interfacial tension on the LAS concentration is shown in Fig. 12(b). The interfacial tensions at the LAS-air and LAS-SO interfaces decreased with an increase in the LAS concentration. Further, we found the inflection point of the slope and estimated the cmc value to be approximately 1 g l^{-1} .

-
- [1] D. Mazumdar and R. I. L. Guthrie, *ISIJ Int.* **35**, 1 (1995).
 [2] S. Kobayashi, *ISIJ Int.* **33**, 577 (1993).
 [3] M. Tanno, J. Liu, X. Gao, S.-J. Kim, S. Ueda, and S.-y. Kitamura, *Metall. Mater. Trans. B* **48**, 2913 (2017).
 [4] G. Kaptay, *Metall. Mater. Trans. B* **32**, 555 (2001).
 [5] L. Champougny, M. Roché, W. Drenckhan, and E. Rio, *Soft Matter* **12**, 5276 (2016).
 [6] S. Natsui, R. Nashimoto, H. Takai, T. Kumagai, T. Kikuchi, and R. O. Suzuki, *Chem. Eng. Sci.* **141**, 342 (2016).
 [7] S. Natsui, R. Nashimoto, D. Nakajima, T. Kumagai, T. Kikuchi, and R. O. Suzuki, *ISIJ Int.* **57**, 394 (2017).
 [8] S. Natsui, R. Nashimoto, H. Takai, T. Kumagai, T. Kikuchi, and R. O. Suzuki, *Metall. Mater. Trans. B* **47**, 1532 (2016).
 [9] G. Debrégeas, P.-G. de Gennes, and F. Brochard-Wyart, *Science* **279**, 1704 (1998).
 [10] J. C. Bird, R. de Ruiter, L. Courbin, and H. A. Stone, *Nature* **465**, 759 (2010).
 [11] L. W. Schwartz and R. V. Roy, *J. Colloid Interface Sci.* **218**, 309 (1999).
 [12] P. D. Howell, *J. Eng. Math.* **35**, 251 (1999).
 [13] P. G. de Gennes, *Langmuir* **17**, 2416 (2001).
 [14] A. Aradian, E. Raphaël, and P.-G. de Gennes, *Europhys. Lett.* **55**, 834 (2001).
 [15] N. Dietrich, S. Poncin, S. Pheulpin, and H. Z. Li, *AIChE J.* **54**, 594 (2008).
 [16] R. Bonhomme, J. Magnaudet, F. Duval, and B. Piar, *J. Fluid Mech.* **707**, 405 (2012).
 [17] K. K. Singh and H.-J. Bart, *Ind. Eng. Chem. Res.* **54**, 9478 (2015).
 [18] G. Reiter and K. Schwerdtfeger, *ISIJ Int.* **32**, 57 (1992).
 [19] J. Liu, S.-j. Kim, X. Gao, S. Uedaz, and S.-y. Kitamura, *ISIJ Int.* **57**, 615 (2017).
 [20] H. Yoshida, J. Liu, S.-J. Kim, X. Gao, S. Ueda, and S.-y. Kitamura, *ISIJ Int.* **56**, 1902 (2016).
 [21] S. Natsui, H. Takai, T. Kumagai, T. Kikuchi, and R. O. Suzuki, *Chem. Eng. Sci.* **111**, 286 (2014).
 [22] S. Natsui, H. Takai, T. Kumagai, T. Kikuchi, and R. O. Suzuki, *Mater. Trans.* **55**, 1707 (2014).
 [23] M. R. Gregory and K. A. Johnston, *N. Z. J. Geol. Geophys.* **30**, 317 (1987).
 [24] M. E. Torresan, USGS Open-File Report No. 87-590 (U.S. Geological Survey, Reston, VA, 1987).
 [25] M. D. Hoover, G. L. Finch, and B. T. Castorina, *J. Aerosol Sci.* **22**, 215 (1991).
 [26] R. Clift, J. R. Grace, and M. E. Weber, *Bubbles, Drops, and Particles* (Dover Publications, Inc., New York, 2005), p. 186.
 [27] F. Pigeonneau and A. Sellier, *Phys. Fluids* **23**, 092102 (2011).
 [28] D. C. Visser, H. C. J. Hoefsloot, and P. D. Iedema, *J. Comput. Phys.* **214**, 491 (2006).
 [29] H. Kočárková, F. Rouyer, and F. Pigeonneau, *Phys. Fluids* **25**, 022105 (2013).
 [30] C. T. Nguyen, H. M. Gonnermann, Y. Chen, C. Huber, A. A. Maiorano, A. Gouldstone, and J. Dufek, *Geochem., Geophys., Geosyst.* **14**, 3616 (2013).
 [31] M. S. Bhamla, C. E. Giacomini, C. Balemans, and G. G. Fuller, *Soft Matter* **10**, 6917 (2014).
 [32] K. J. Mysels, K. Shinoda, and S. Frankel, *Soap Films: Studies of Their Thinning* (Pergamon Press, London, 1959).
 [33] L. Saulnier, L. Champougny, G. Bastien, F. Restagno, D. Langevin, and E. Rio, *Soft Matter* **10**, 2899 (2014).
 [34] H. Lhuissier and E. Villermaux, *J. Fluid Mech.* **696**, 5 (2012).
 [35] D. E. Spiel, *J. Geophys. Res.* **103**, 24907 (1998).
 [36] J. M. Andreas, E. A. Hauser, and W. B. Tucker, *J. Phys. Chem.* **42**, 1001 (1938).